AIAA JOURNAL
Vol. 39, No. 2, February 2001

Harmonic Finite Element Analysis for Anisotropic Viscoelasticity

Omri Rand* and Dan Givoli*
Technion—Israel Institute of Technology, 32000 Haifa, Israel

A numerical methodology for predicting the linear anisotropic viscoelastic behavior of bodies that can be uniquely described in cylindrical coordinates is devised. The methodology is an extension of the Fourier–finite element method and is based on a combination of finite element discretization in the radial and longitudinal directions and Fourier decomposition in the angular direction. The proposed method is capable of handling inhomogeneous polar-orthotropic viscoelastic material properties. In general, the method provides dimensional reduction in the finite element formulation, which leads to a reduction in the complexity of the numerical model including the meshing process. Overall, the method is shown to be competent mainly because of the efficient exploitation of the angular description of the geometry and the properties distribution. A numerical example is given for the analysis of an orthotropic viscoelastic ring under asymmetric shear loading.

Introduction

FOURIER decomposition is a well-established analytical tool that has been proved to be efficient in a vast range of engineering applications where one or more of the problem dimensions exhibits periodicity. Classical dynamic problems were treated using Fourier decomposition in time, whereas the other (spatial) dimensions were treated differently (see e.g., Refs. 1–4). In other cases where the structure exhibits axisymmetric geometry, Fourier decomposition can be exploited by its application to the periodic loading. Typical examples are classical analyses of cylindrical shells where the circumferential directions can be described using Fourier decomposition (see, e.g., Refs. 5–9) or modern long space structures that exhibit periodicity in the longitudinal distribution of their dynamic and structural properties. In general, it can be shown that Fourier analysis is efficient where "smooth" variations are under discussion, while its attractiveness is reduced as the variations become more abrupt and sharp.

One of the common combinations of Fourier decomposition with other discretization methods is its combination with the finite element analysis, see, e.g., linear analyses in Refs. 10–14 and nonlinear analyses in Refs. 15–18. One class of such finite elements methods are finite strip methods, see, e.g., Refs. 19 and references therein. As already mentioned, in many cases, such Fourier–finite element (FFE) methods have been applied to bodies of revolution that undergo asymmetric loading. In such cases the loads are expanded into their Fourier-series coefficients of the deformation at each node. Subsequently, these Fourier-series coefficients become the problem unknowns. In a linear system a separate solution for each harmonic can be executed, and later on, any loading variation can be applied and the elastic response can be constructed using superposition.

Reference 20 presents a further discussion of the characteristics of the FFE method and a unique version of it for nonlinear heat-transfer problems. The method is based on a nonstandard variational (virtual-work) form of the problem and finite element formulation in cylindrical coordinates. The analysis leads to a system of semidiscrete equations with respect to the angular direction. The resulting equations are periodic with respect to the cylindrical coordinate angle. These equations are then solved using a special-purpose symbolic manipulation tool[21] that ensures harmonic–balance type of solution up to a required finite number of harmonics. This FFE method easily handles asymmetric geometries, namely domains that deviate from bodies of revolution. The only theoretical geometric restriction is that the inner and outer boundaries of the given body can be defined continuously and uniquely in cylindrical coordinates. In addition, the thermal material properties are also allowed to be asymmetric provided that they may be uniquely described in cylindrical coordinates.

The preceding FFE method is extended in the present paper to the context of the linear elastic behavior of a solid body. Unlike the thermal analysis demonstrated in Ref. 20, the present case, which is derived for materials with polar orthotropy, includes two (coupled) components of the elastic displacement at each point (compared with a single temperature unknown in the thermal analysis). The extension therefore includes a suitable finite element discretization, while the harmonic balancing procedure is applied to both the radial and circumferential deformation components.

Once a static solution procedure is presented, the analysis is applied to the case of viscoelastic materials, which are analyzed using a complex representation of the elastic moduli. From a practical point of view, this extension doubles the problem size and requires simultaneous coupled solution of the doubled system. To overcome this difficulty, an efficient iterative solution, which requires minor changes in the formulation, is discussed and demonstrated.

The present extension of the FFE methodology establishes a method that compliments the thermal analysis of Ref. 20. In other words, it enables a complete thermoelastic analysis where the two models are employed in a sequential manner. Engineering applications of such thermoelastic analysis include stationary and rotating discs, shafts and wheels, solid-fuel engines, and elements of space structures, which are exposed to periodic incoming solar heat flux. In each of these cases, the proposed methodology is capable of handling the periodicity in loading, geometry, and properties distribution.

To demonstrate the present methodology features, the formulation presented in this case is restricted to the case of two-dimensional elasticity. Yet, adding the third longitudinal coordinate requires a minor additional effort and can be carried out along the lines presented in what follows.

The theoretical and computational aspects of the proposed FFE method are discussed in details in Ref. 20 in the context of nonlinear heat problems. The current extension to elastic and viscoelastic problems is technically more involved because of the tensorial nature of the equations, but all of the numerical properties of the approach are retained. Reference 20 includes verification of the approach and discussion on its accuracy, efficiency, and convergence.

Finite Element Formulation

Consider the equations of two-dimensional linear elasticity in polar coordinates for a material with polar orthotropy (see Fig. 1a). The differential equilibrium equations for the stresses σ_{ij} in this case are

$$\sigma_{rr,r} + (1/r)\sigma_{r\theta,\theta} + (\sigma_{rr} - \sigma_{\theta\theta}/r) + F_r = 0 \tag{1a}$$

$$\sigma_{r\theta,r} + (1/r)\sigma_{\theta\theta,\theta} + 2(\sigma_{r\theta}/r) + F_\theta = 0 \tag{1b}$$

Received 25 May 1999; revision received 30 April 2000; accepted for publication 26 June 2000.

*Associate Professor, Faculty of Aerospace Engineering and Asher Center for Space Research.

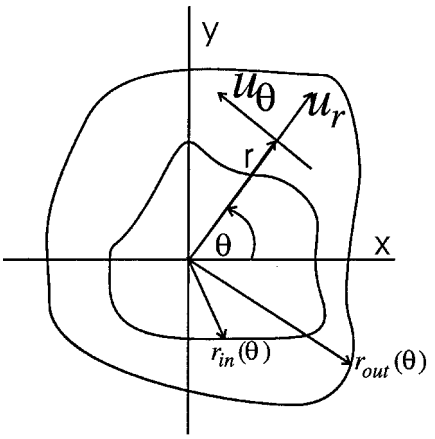

Fig. 1a Polar coordinates notation.

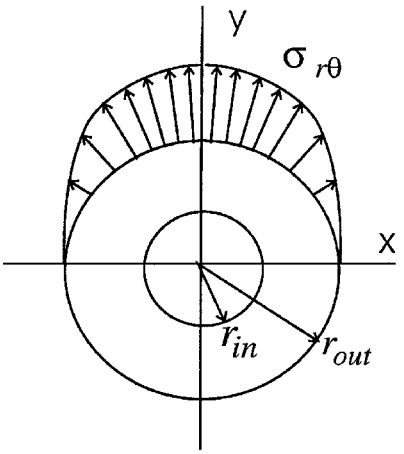

Fig. 1b Isotropic circular ring undergoing a sine distribution of shear-stress loading along half of its outer circumference.

where r and θ are the radial and tangential polar coordinates, respectively, and F_r and F_θ are the radial and tangential body force components, respectively. Here, a comma indicates partial differentiation. The involved strains are given by

$$\epsilon_{rr} = u_{r,r} \tag{2a}$$

$$\epsilon_{\theta\theta} = (1/r)u_{\theta,\theta} + (u_r/r) \tag{2b}$$

$$\epsilon_{r\theta} = \tfrac{1}{2}[(1/r)u_{r,\theta} + u_{\theta,r} - (u_\theta/r)] \tag{2c}$$

where u_r and u_θ are the radial and tangential displacements, respectively (Fig. 1a). The constitutive relations in this case can be written as

$$\begin{Bmatrix} \sigma_{rr} \\ \sigma_{\theta\theta} \\ \sigma_{r\theta} \end{Bmatrix} = \begin{bmatrix} C_{rr} & C_{r\theta} & 0 \\ C_{r\theta} & C_{\theta\theta} & 0 \\ 0 & 0 & 2G \end{bmatrix} \begin{Bmatrix} \epsilon_{rr} \\ \epsilon_{\theta\theta} \\ \epsilon_{r\theta} \end{Bmatrix} \tag{3}$$

C_{rr}, $C_{r\theta}$, $C_{\theta\theta}$, and G are the elastic moduli. In a polar-orthotropic material the latter four moduli are independent. In an isotropic material $C_{rr} = C_{\theta\theta}$ and $2G = C_{rr} - C_{r\theta}$ so that there are only two independent moduli.

We write these equations in a symmetric weak form, where the variable r is treated variationally, whereas θ is unaffected. To this end, we multiply Eqs. (1a) and (1b) by the test functions $w_r(r)$ and $-w_\theta(r)$, respectively, sum them together, and integrate over the interval $[r_{\text{in}}, r_{\text{out}}]$. Then we integrate by parts some of the terms and use Eqs. (2a–2c) and Eq. (3). This yields

$$\begin{aligned}\int_{r_{\text{in}}}^{r_{\text{out}}} \Bigg\{ & w_r' r C_{rr} u_r' + C_{r\theta}(w_r' \dot{u}_\theta + w_\theta' \dot{u}_r') + C_{r\theta}(w_r' u_r + w_r u_r') \\ & - w_r \left(\frac{G}{r}\right) \ddot{u}_r - G(w_r \dot{u}_\theta' + w_\theta' \dot{u}_r) + \left[\frac{(G + C_{\theta\theta})}{r}\right] \\ & \times (w_r \dot{u}_\theta + w_\theta \dot{u}_r) + w_r \left(\frac{C_{\theta\theta}}{r}\right) u_r - w_\theta' r G u_\theta' \\ & + G(w_\theta' u_\theta + w_\theta u_\theta') - w_\theta \left(\frac{G}{r}\right) u_\theta + w_\theta \left(\frac{C_{\theta\theta}}{r}\right) \ddot{u}_\theta \\ & + E(r, \theta) \Bigg\} \, \mathrm{d}r = (w_r r \sigma_{rr} - w_\theta r \sigma_{r\theta})_{r_{\text{in}}}^{r_{\text{out}}} \\ & + \int_{r_{\text{in}}}^{r_{\text{out}}} (w_r F_r - w_\theta F_\theta) r \, \mathrm{d}r \end{aligned} \tag{4}$$

Here a prime denotes differentiation with respect to r, and a superposed dot denotes differentiation with respect to θ. $E(r, \theta)$ is a correction term that should be added in cases where the geometry is not axisymmetric. This correction reflects the additional terms that are required when the partial derivatives with respect to θ are carried out along a line for which r is not constant (see Ref. 20 for more details).

To obtain the finite element formulation, we now expand u_r and u_θ in finite element shape functions, i.e., in each element

$$u_r(r, \theta) = \sum_a N_a^r(r) d_a^r(\theta), \qquad u_\theta(r, \theta) = \sum_a N_a^\theta(r) d_a^\theta(\theta) \tag{5}$$

Here a is the index associated with node a of the element, and d_a^r and d_a^θ are the unknown nodal displacements. In general, the shape functions N_a^r and N_a^θ may be different, although it is convenient to choose $N_a^r = N_a^\theta$. Using the Galerkin procedure, we also expand w_r and w_θ in terms of N_a^r and N_a^θ, respectively. Then we substitute all these expressions in Eq. (4) and make use of the arbitrariness of the test functions. This finally results in the system of ordinary differential equations:

$$\boldsymbol{M}\boldsymbol{d}_{,\theta\theta}(\theta) + \boldsymbol{C}\boldsymbol{d}_{,\theta}(\theta) + \boldsymbol{K}\boldsymbol{d}(\theta) = \boldsymbol{F}(\theta) \tag{6}$$

Here $\boldsymbol{d}(\theta)$ is the unknown vector whose entries include d_a^r and d_a^θ. This system has a similar form to that obtained in transient analysis, although in the latter context a superposed dot denotes differentiation with respect to time rather than with respect to the angle θ.

The expressions for the entries of the matrices $\boldsymbol{M}$, $\boldsymbol{C}$, and $\boldsymbol{K}$ and the vector $\boldsymbol{F}$ are given on the element level by

$$m_{ab}^{rr} = -\int_{\Omega^e} N_a^r \left(\frac{G}{r}\right) N_b^r \, \mathrm{d}\Omega \tag{7a}$$

$$m_{ab}^{\theta\theta} = \int_{\Omega^e} N_a^\theta \left(\frac{C_{\theta\theta}}{r}\right) N_b^\theta \, \mathrm{d}\Omega \tag{7b}$$

$$m_{ab}^{r\theta} = m_{ab}^{\theta r} = 0 \tag{7c}$$

$$c_{ab}^{rr} = c_{ab}^{\theta\theta} = 0 \tag{7d}$$

$$c_{ab}^{r\theta} = \int_{\Omega^e} \left\{ N_a^{r\prime} C_{r\theta} N_b^\theta - N_a^r G N_b^{\theta\prime} + N_a^r \left[\frac{(G + C_{\theta\theta})}{r}\right] N_b^\theta \right\} \mathrm{d}\Omega \tag{7e}$$

$$c_{ab}^{\theta r} = \int_{\Omega^e} \left\{ N_a^\theta C_{r\theta} N_b^{r\prime} - N_a^{\theta\prime} G N_b^r + N_a^\theta \left[\frac{(G + C_{\theta\theta})}{r}\right] N_b^r \right\} \mathrm{d}\Omega \tag{7f}$$

$$\begin{aligned} k_{ab}^{rr} = \int_{\Omega^e} \Bigg[& N_a^{r\prime} r C_{rr} N_b^{r\prime} + C_{r\theta}\left(N_a^{r\prime} N_b^r + N_a^r N_b^{r\prime}\right) \\ & + N_a^r \left(\frac{C_{\theta\theta}}{r}\right) N_b^r \Bigg] \mathrm{d}\Omega \end{aligned} \tag{7g}$$

$$k_{ab}^{\theta\theta} = \int_{\Omega^e} \left[-N_a^{\theta\prime} r G N_b^{\theta\prime} + G\left(N_a^{\theta\prime} N_b^{\theta} + N_a^{\theta} N_b^{\theta\prime}\right) - N_a^{\theta}\left(\frac{G}{r}\right) N_b^{\theta} \right] \mathrm{d}\Omega \tag{7h}$$

$$k_{ab}^{r\theta} = k_{ab}^{\theta r} = 0 \tag{7i}$$

$$f_a^r = \int_{\Omega^e} N_a^r F_r r \, \mathrm{d}\Omega + \beta_{\text{out}}^a r_{\text{out}} (\sigma_{rr})_{\text{out}} - \beta_{\text{in}}^a r_{\text{in}} (\sigma_{rr})_{\text{in}} \tag{7j}$$

$$f_a^\theta = -\int_{\Omega^e} N_a^\theta F_\theta r \, \mathrm{d}\Omega - \beta_{\text{out}}^a r_{\text{out}} (\sigma_{r\theta})_{\text{out}} - \beta_{\text{in}}^a r_{\text{in}} (\sigma_{r\theta})_{\text{in}} \tag{7k}$$

Here m_{ab}^{ij}, c_{ab}^{ij}, k_{ab}^{ij}, and f_a^i are the element-level counterparts of the global matrices and vector $\boldsymbol{M}$, $\boldsymbol{C}$, $\boldsymbol{K}$, and $\boldsymbol{F}$, respectively, and Ω^e is the r domain of the element. From Eqs. (7a–7i) it can be easily verified that $\boldsymbol{M}$, $\boldsymbol{C}$, and $\boldsymbol{K}$ are symmetric matrices. In Eqs. (7j) and (7k), β_{out}^a is defined as 1 if node a is at $r = r_{\text{out}}$ and is loaded by traction and as 0 otherwise, similarly for β_{in}^a. Also, $(\sigma_{rr})_{\text{out}}$, $(\sigma_{rr})_{\text{in}}$, $(\sigma_{r\theta})_{\text{out}}$, and $(\sigma_{r\theta})_{\text{in}}$ are the prescribed traction values at the two edges.

Fourier Decomposition

At this stage the unknown nodal displacements d_a^r and d_a^θ are expressed by their Fourier sine and cosine coefficients, namely,

$$d_a^r(\theta) = d_{a0}^r + \sum_{n=1}^{N_\theta} d_{ac}^r(n)\cos(n\theta) + d_{as}^r(n)\sin(n\theta) \tag{8a}$$

$$d_a^\theta(\theta) = d_{a0}^\theta + \sum_{n=1}^{N_\theta} d_{ac}^\theta(n)\cos(n\theta) + d_{as}^\theta(n)\sin(n\theta) \tag{8b}$$

Substitution of Eqs. (8a) and (8b) in Eq. (6) including their derivatives with respect to θ yields a linear system of $2(2N_\theta + 1)N_r$ equations and unknowns (where N_r is the number of radial nodes). In the general case the matrices $\boldsymbol{M}$, $\boldsymbol{C}$, and $\boldsymbol{K}$ are functions of θ as a result of the asymmetry of the geometry and material properties, and, therefore, the harmonics of the resulting system are fully coupled. In the later case the construction of the linear system is a straightforward but tedious (algebraic and trigonometric) task to which a considerable analytic effort should be devoted. This task is therefore carried out using the special-purpose symbolic analytic tools reported in Ref. 21. The end result of this step is a linear algebraic system of equations for the unknown vector:

$$\left\langle d_{a0}^r, d_{a0}^\theta, d_{ac}^r(1), d_{as}^r(1), d_{ac}^\theta(1), d_{as}^\theta(1), \ldots, d_{ac}^r(N_\theta), d_{as}^r(N_\theta), d_{ac}^\theta(N_\theta), d_{as}^\theta(N_\theta) \right\rangle^T$$

Viscoelastic Materials

The extension of the present formulation to the case of viscoelastic materials is based on the common complex representation of these materials (see, e.g., Ref. 22). Subsequently, the elastic moduli C_{ij} and G [see Eq. (3)] are replaced by $C_{ij}^R + iC_{ij}^I$ and $G^R + iG^I$, respectively, where $i = \sqrt{-1}$. C_{ij}^R and G^R are usually referred to as the storage moduli, whereas C_{ij}^I and G^I are known as the loss moduli. Accordingly, the matrices $\boldsymbol{M}$, $\boldsymbol{C}$, and $\boldsymbol{K}$ become complex as well, and Eq. (6) can be written as

$$[\boldsymbol{M}^R + i\boldsymbol{M}^I]\{\boldsymbol{d}^R + i\boldsymbol{d}^I\}_{,\theta\theta} + [\boldsymbol{C}^R + i\boldsymbol{C}^I]\{\boldsymbol{d}^R + i\boldsymbol{d}^I\}_{,\theta} + [\boldsymbol{K}^R + i\boldsymbol{K}^I]\{\boldsymbol{d}^R + i\boldsymbol{d}^I\} = \{\boldsymbol{F}^R + i\boldsymbol{F}^I\} \tag{9}$$

It is now possible to balance the imaginary and real parts of Eq. (9) separately. This yields

$$\boldsymbol{M}^R\boldsymbol{d}_{,\theta\theta}^R + \boldsymbol{C}^R\boldsymbol{d}_{,\theta}^R + \boldsymbol{K}^R\boldsymbol{d}^R = \boldsymbol{M}^I\boldsymbol{d}_{,\theta\theta}^I + \boldsymbol{C}^I\boldsymbol{d}_{,\theta}^I + \boldsymbol{K}^I\boldsymbol{d}^I + \boldsymbol{F}^R \tag{10a}$$

$$\boldsymbol{M}^R\boldsymbol{d}_{,\theta\theta}^I + \boldsymbol{C}^R\boldsymbol{d}_{,\theta}^I + \boldsymbol{K}^R\boldsymbol{d}^I = -\boldsymbol{M}^I\boldsymbol{d}_{,\theta\theta}^R - \boldsymbol{C}^I\boldsymbol{d}_{,\theta}^R - \boldsymbol{K}^I\boldsymbol{d}^R + \boldsymbol{F}^I \tag{10b}$$

As shown, each one of Eqs. (10a) and (10b) constitutes the same system (the left-hand sides of the equations) with different loading (the right-hand sides of the equations). Thus, sequential solution of Eqs. (10a) and (10b) requires a solution of the same system (i.e., the same inverse matrix is maintained throughout the entire solution) with different loading vectors. The process is initiated by an initial guess (usually zero) for $\boldsymbol{d}^I$, which is substituted in the right-hand side (RHS) of Eq. (10a). Then, $\boldsymbol{d}^R$ is determined and substituted in the RHS of Eq. (10b), the solution of which yields a corrected value for $\boldsymbol{d}^I$. The process is repeated until convergence is achieved.

Typically, the imaginary parts of the complex elastic moduli are small compared with the real parts. Properties of representative isotropic and composite materials are documented in Ref. 22. It is common to define the material loss factors as the ratio of the loss moduli and the storage moduli, namely, $\eta_{ij} = C_{ij}^I / C_{ij}^R$ and $\eta_G = G^I / G^R$. As shown in Ref. 22, the loss factors reach values of only few percent. These typical values give rise to the excellent convergence properties of the iterative scheme just described.

Illustrative Results

Figure 1b presents a circular ring undergoing a distribution of shear stress $\sigma_{r\theta}$ along half of its outer circumference given by

$$\sigma_{r\theta} = \begin{cases} \bar{\sigma}_{r\theta}\sin\theta & \text{for} \quad 0 < \theta < \pi \\ 0 & \text{for} \quad \pi \le \theta \le 2\pi \end{cases}$$

A systematic convergence study has shown that 10 harmonics are sufficient for describing the response for the load under discussion, and additional terms do not contribute any meaningful changes.

The preceding load distribution has been applied to the outer circumference of an isotropic concentric circular ring of $r_{\text{out}}/r_{\text{in}} = 1.67$. The inner boundary was assumed to be fixed, namely, $u_r = u_\theta = 0$ for $r = r_{\text{in}}$. The loss factors in this case were assumed to be $\eta_E = \eta_G = 0.1$ (obviously, these values need not be equal, and this selection is for illustration purposes only). The radial direction has been divided into nine equal elements (i.e., 10 nodes where node 1 coincides with $r = r_{\text{in}}$ and node 10 coincides with $r = r_{\text{out}}$). Therefore, the present analysis includes $2(2N_\theta + 1)N_r = 420$ unknowns (including boundary nodes).

Figure 2 presents the real component of the displacements per unit shear-stress magnitude $\bar{\sigma}_{r\theta}$ at some radial locations vs the angular coordinates θ. The corresponding imaginary parts are shown

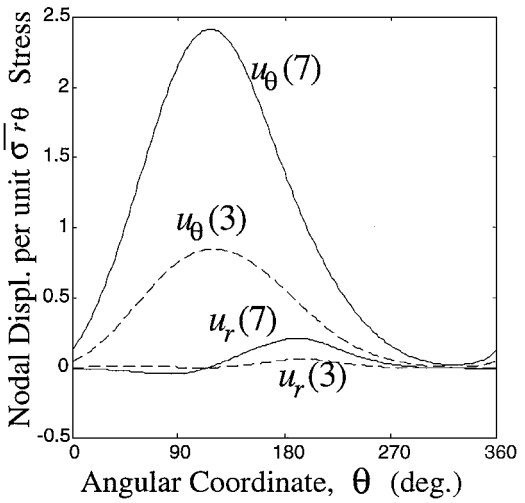

Fig. 2 Real component of the displacements per unit $\bar{\sigma}_{r\theta}$ shear stress at some radial locations vs the angular coordinates θ.

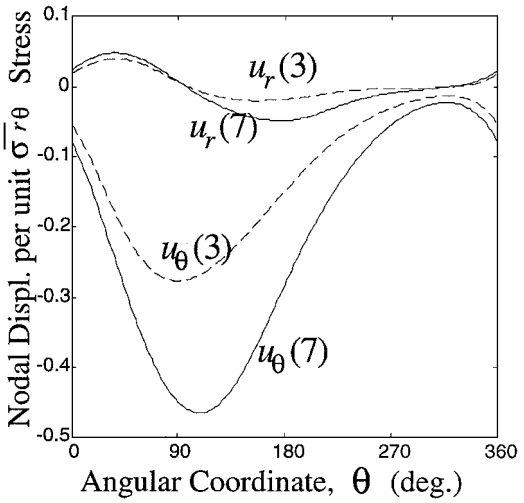

Fig. 3 Imaginary component of the displacements per unit $\bar{\sigma}_{r\theta}$ shear stress at some radial locations vs the angular coordinates θ.

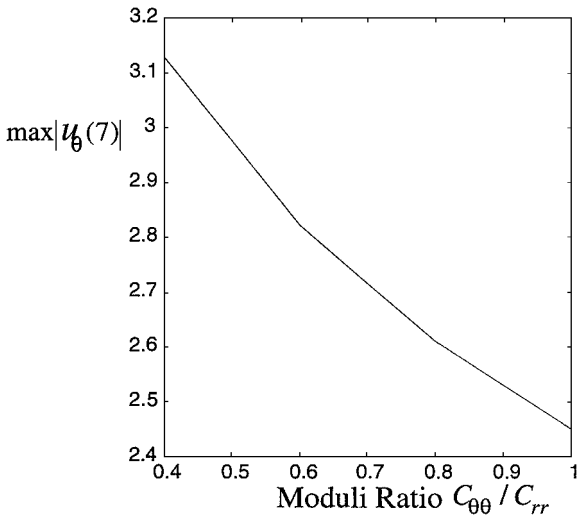

Fig. 4 Maximal absolute value of $u_\theta(7)$ per unit $\bar{\sigma}_{r\theta}$ as a function of the $C_{\theta\theta}/C_{rr}$ ratio (C_{rr} and G are constants). The case of $C_{\theta\theta}/C_{rr} = 1$ corresponds to the isotropic case.

in Fig. 3. All of the displacements shown are normalized with respect to $r = r_{\text{in}}$. As shown, the magnitude of the displacements u_θ is higher closer to the loaded outer boundary, whereas the absolute magnitudes of the imaginary parts are roughly only 20% of the corresponding real parts. The sharpness of the loading variation is smeared as the radial distance from the outer surface is increased.

Orthotropy effects for this case are presented in Fig. 4, where the maximal absolute value of u_θ at radial node 7 per unit $\bar{\sigma}_{r\theta}$ is plotted as a function of the $C_{\theta\theta}/C_{rr}$ ratio [see Eq. (3)]. In this case $\eta_{ij} = \eta_G = 0.05$ were assumed. As shown, the maximal value of the preceding radial displacement grows while the moduli ratio is decreased, and for typical orthotropic material this value can be substantially larger then the one obtained for the isotropic case $C_{\theta\theta}/C_{rr} = 1$.

Summary

An extension of the FFE method, which is tailored for the linear elastic and viscoelastic analysis of bodies that may be described in cylindrical coordinates, has been presented. The method combines a finite element discretization in the radial and the longitudinal directions and Fourier decomposition in the angular direction. The method is capable of handling inhomogeneous polar-orthotropic material properties and enables dimensional reduction of the standard finite element formulation. The efficiency of the method was demonstrated by few numerical examples of linear plane orthotropic viscoelasticity.

Extensive numerical experimentation, performed in the elastic case but not presented here, shows that the present method is more efficient than the standard finite element method when the loading is relatively smooth with respect to the angular coordinate, whereas the opposite is true for sharp angular changes. This is caused by the increasing number of harmonics that are required for sharp loading distributions.

Acknowledgment

This work was supported by the Adler Fund managed by the Israel Academy of Sciences.

References

[1] Kalinowski, A. J., and Wachman, M., "Combined Finite Element Method and Spectral Method for Shear Flow-Structure Interaction Problems," *Proceedings of the ASME Winter Annual Meeting*, Vol. 178, American Society of Mechanical Engineers, New York, 1993, pp. 65–79.

[2] Kohl, T., Datta, S. K., and Shah, A. H., "Axially Symmetric Pulse Propagation in Semi-Infinite Hollow Cylinders," *AIAA Journal*, Vol. 30, No. 6, 1992, pp. 1617–1624.

[3] Rand, O., "Periodic Response of Thin-Walled Composite Helicopter Rotor Blades," *Journal of the American Helicopter Society*, Vol. 36, No. 4, 1991, pp. 3–11.

[4] Rand, O., and Givoli, D., "A Finite Element Spectral Method with Application to the Thermoelastic Analysis of Space Structures," *International Journal of Numerical Methods in Engineering*, Vol. 30, No. 2, 1990, pp. 291–306.

[5] Ding, W., and Xu, J., "Stability Analysis of Laminated and Stiffened Composite Shells of Revolution by the Finite Element Method," *Journal of Strain Analysis for Engineering Design*, Vol. 25, No. 3, 1990, pp. 151–156.

[6] Calladine, C. R., *Theory of Shell Structures*, Cambridge Univ. Press, Cambridge, England, U.K., 1983, pp. 59–67.

[7] Axelrad, E. L., and Emmerling, F. A., "Elastic Tubes," *Applied Mechanics Reviews*, Vol. 37, No. 7, July 1984, pp. 891–897.

[8] Fosberg, K., "A Review of Analytical Methods Used to Determine the Modal Characteristics of Cylindrical Shells," NASA CR 613, Sept. 1966.

[9] Brush, D. O., and Almroth, B. O., *Buckling of Bars, Plates, and Shells*, International Student ed., McGraw-Hill, Kogakusha Ltd., Tokyo, 1975, pp. 190–224.

[10] Amon, C. H., "Spectral Element-Fourier Method for Transitional Flows in Complex Geometries," *AIAA Journal*, Vol. 31, No. 1, 1993, p. 42.

[11] Kim, J. R., Kim, W. D., and Kim, S. J., "Parallel Computing Using Semianalytical Finite Element Method," *AIAA Journal*, Vol. 32, No. 5, 1994, pp. 1066–1071.

[12] Thurston, G. A., and Sistla, R., "Elimination of Gibbs' Phenomena from Error Analysis of Finite Element Results," *AIAA Journal*, Vol. 29, No. 12, 1991, pp. 2233–2239.

[13] Kumar, V., and Singh, A. V., "Approximate Vibrational Analysis of Noncircular Cylinders Having Varying Thickness," *AIAA Journal*, Vol. 30, No. 7, 1992, pp. 1929–1931.

[14] Givoli, D., and Rand, O., "Harmonic Finite Element Thermoelastic Analysis of Space Frames and Trusses," *Journal of Thermal Stresses*, Vol. 16, No. 3, 1993, pp. 233–248.

[15] Kaiser, T. M. V., Elwi, A. E., and Mioduchowski, A., "Nonlinear Harmonic Analysis Applied to Axisymmetric Structures," *Computers and Structures*, Vol. 55, No. 6, 1995, pp. 1107–1118.

[16] Danielson, K. T., and Tielking, J. T., "Fourier Continuum Finite Elements for Large Deformation Problems," *Computers and Structures*, Vol. 49, No. 1, 1993, pp. 133–147.

[17] Marusak, R. E., and Becker, E. B., "Finite Element Procedure for Axisymmetric Elastomeric Solids Under General Loading," *International Journal for Numerical Methods in Engineering*, Vol. 36, No. 12, 1993, pp. 2031–2048.

[18] Givoli, D., and Rand, O., "Thermoelastic Analysis of Space Structures in Periodic Motion," *AIAA Journal of Spacecraft and Rockets*, Vol. 28, No. 4, 1991, pp. 457–464.

[19] Cheung, Y. K., and Tham, L. G., *Finite Strip Method*, CRC Press, London, 1998.

[20] Givoli, D., and Rand, O., "A Generalized Finite Element-Harmonic Analysis for Nonlinear Heat Transfer," *Journal of Thermophysics and Heat Transfer*, Vol. 13, No. 1, 1999, pp. 100–109.

[21] Rand, O., "Harmonic Variables—A New Approach to Nonlinear Periodic Problems," *Journal of Computers and Mathematics with Applications*, Vol. 15, No. 11, 1988, pp. 953–961.

[22] Sun, C. T., and Lu, Y. P., *Vibration Damping of Structural Element*, Prentice–Hall, Upper Saddle River, NJ, 1995, Chaps. 1, 2.

S. Saigal
Associate Editor